Water Splitting

International Edition: DOI: 10.1002/anie.201700150
German Edition: DOI: 10.1002/ange.201700150

# Noble-Metal-Free Janus-like Structures by Cation Exchange for Z-Scheme Photocatalytic Water Splitting under Broadband Light Irradiation

*Qichen Yuan[+], Dong Liu[+], Ning Zhang, Wei Ye, Huanxin Ju, Lei Shi, Ran Long, Junfa Zhu, and Yujie Xiong**

***Abstract:*** *Z-scheme water splitting is a promising approach based on high-performance photocatalysis by harvesting broadband solar energy. Its efficiency depends on the well-defined interfaces between two semiconductors for the charge kinetics and their exposed surfaces for chemical reactions. Herein, we report a facile cation-exchange approach to obtain compounds with both properties without the need for noble metals by forming Janus-like structures consisting of γ-MnS and $Cu_7S_4$ with high-quality interfaces. The Janus-like γ-MnS/$Cu_7S_4$ structures displayed dramatically enhanced photocatalytic hydrogen production rates of up to 718 $\mu mol\, g^{-1} h^{-1}$ under full-spectrum irradiation. Upon further integration with an $MnO_x$ oxygen-evolution cocatalyst, overall water splitting was accomplished with the Janus structures. This work provides insight into the surface and interface design of hybrid photocatalysts, and offers a noble-metal-free approach to broadband photocatalytic hydrogen production.*

The global energy demand calls for the development of new sustainable energy technologies. Among them, photocatalytic water splitting, which harvests solar light to produce $H_2$ and $O_2$, is a promising approach to the conversion of solar into hydrogen energy.[1,2] The main obstacle to progress in this field has been the lack of a suitable photocatalyst that meets the following four requirements: 1) Harvesting and utilization of broadband light, 2) efficient separation and transfer of electron–hole pairs, 3) sufficient band-edge potentials for overall water splitting, and 4) low material costs. To address these four requirements, innovation in terms of material design and the development of new synthetic methods are required.[3,4]

To meet these demanding goals, drawing inspiration from nature,[5] various all-solid-state artificial Z-scheme photocatalytic systems have been developed based on two semiconductors that possess band structures with a staggered alignment and different band gaps.[6–17] These systems not only offer complementary light absorption in different spectral regions and spatial separation of electrons from holes, but also maintain the energy levels of the remaining electrons and holes for sufficient reactivity, which can hardly be attained with other designs.[18] Given the working mechanism, an ideal Z-scheme system should possess two structural characteristics: 1) Well-defined interfaces for efficient interfacial charge transfer and 2) exposed surfaces on both semiconductors for reduction and oxidation half-reactions on the surfaces.[18] To reduce the material costs, noble metals, which are commonly used as electron mediators (e.g., Au, Ag, and Ir) to facilitate the charge transfer between semiconductors in Z-scheme water splitting or as cocatalysts (e.g., Rh and Pt) to promote $H_2$ evolution,[6–8,10] should ideally be excluded from the interfaces. The exclusion of noble metals from Z-scheme water splitting systems can also avoid the possible backward reaction of $O_2$ and $H_2$ on the metal surface to give water.[19]

Herein, we report a cation-exchange approach to Janus-like structures that enables the exposure of both semiconductor components, namely roxbyite $Cu_7S_4$ and γ-MnS, on the surface towards broadband photocatalytic $H_2$ production. The cation exchange provides a versatile approach for forming high-quality interfacial contacts between the semiconductors with atomic precision.[20] By controlling the constituents involved in the synthesis (i.e., the initial templates and incoming cations), distinctly immiscible domains can be integrated in situ, in a smoother fashion than with most postsynthetic treatments of colloidal nanocrystals.[21]

In our work, we selected roxbyite $Cu_7S_4$ nanocrystals as the starting templates owing to their high density of Cu vacancies, which facilitate cation exchange.[22] The challenge that we faced with our system was to rationally form Janus structures by excluding another immiscible phase, namely core–shell structures. To this end, tetrahedrally coordinated $Mn^{2+}$ ions were chosen as the incorporated cations[23] as tetrahedrally coordinated cations have great potential to coexist with copper chalcogenide nanocrystals in a Janus-like form.[24] In terms of their band structures, roxbyite $Cu_7S_4$ and γ-MnS display a staggered alignment and absorb near-infrared (NIR) and ultraviolet/visible (UV/Vis) light, respectively.[25–28] Moreover, the surface plasmons of $Cu_7S_4$ can make an additional contribution to light harvesting.[29]

As illustrated in Figure 1a, we first synthesized roxbyite $Cu_7S_4$ nanocrystals (NC1) with a hexagonal-bipyramidal

[*] Q. Yuan,[+] D. Liu,[+] N. Zhang, Dr. W. Ye, Dr. H. Ju, L. Shi, Dr. R. Long, Prof. J. Zhu, Prof. Y. Xiong
Hefei National Laboratory for Physical Sciences at the Microscale
iChEM (Collaborative Innovation Center of Chemistry for Energy Materials), School of Chemistry and Materials Science and National Synchrotron Radiation Laboratory
University of Science and Technology of China
Hefei, Anhui 230026 (P.R. China)
E-mail: yjxiong@ustc.edu.cn
[+] These authors contributed equally to this work.
Supporting information and the ORCID identification number(s) for the author(s) of this article can be found under: http://dx.doi.org/10.1002/anie.201700150.

  

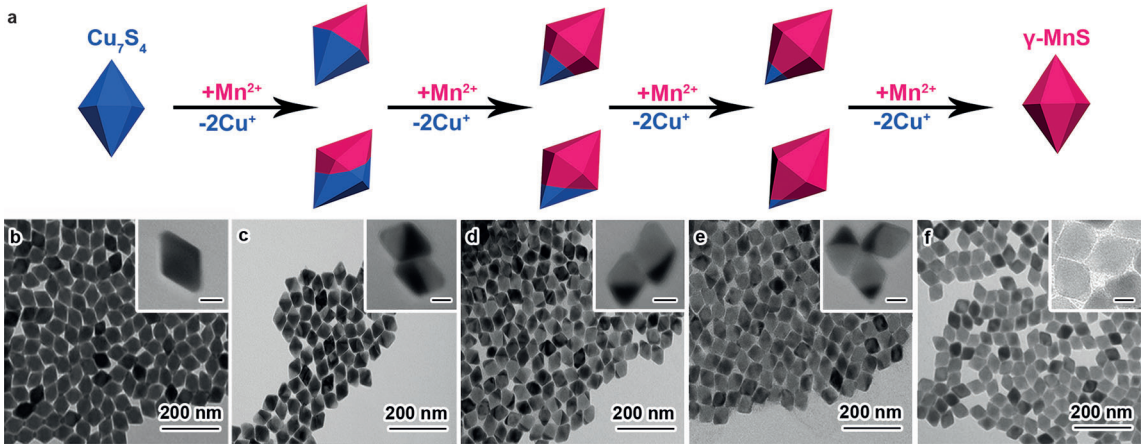


***Figure 1.*** Cation exchange evolution by precisely controlling the reaction time. a) Schematic illustration of the cation exchange process. TEM images of b) the initial roxbyite $Cu_7S_4$ nanocrystals (NC1), c) a γ-MnS/$Cu_7S_4$ sample after cation exchange for 0.5 h (NC2), d) a γ-MnS/$Cu_7S_4$ sample after cation exchange for 1 h (NC3), e) a γ-MnS/$Cu_7S_4$ sample after cation exchange for 1.5 h (NC4), and f) the γ-MnS sample after nearly complete cation exchange (NC5). Scale bars: 25 nm.

morphology, and used them as the starting templates for the cation exchange from $Cu_7S_4$ to γ-MnS. This transformation was carefully controlled to produce a series of samples with various Mn/Cu ratios (NC2–NC5) by changing the time and temperature of the cation exchange. As indicated by inductively coupled plasma mass spectrometry (ICP-MS; see the Supporting Information, Table S1), the Mn/Cu molar ratios of NC2–NC4 were 0.6, 3, and 6, respectively. An NC5 sample with a Mn/Cu molar ratio of up to 256 was eventually obtained after nearly complete cation exchange at a higher temperature and with a longer reaction time, which can roughly be regarded as γ-MnS nanocrystals.

Transmission electron microscopy (TEM) images (Figure 1 b–f) clearly show the heterogeneous interfaces in the NC2, NC3, and NC4 samples, which cannot be observed in the initial template NC1 and the completely cation-exchanged sample NC5. The dynamic process for interface evolution, which leads to the formation of Janus-like nanocrystals, is illustrated in Movie S1. This results confirms our hypothesis that the tetrahedrally coordinated $Mn^{2+}$ ions can induce the formation of Janus-like structures through cation exchange.

Despite their different chemical compositions, the samples well inherited the geometrical shape of the initial templates as revealed by scanning electron microscopy (SEM; Figure S1). This suggests that the cation exchange process is well controlled in our synthesis.[30,31] It is worth pointing out that the NC5 (the completely cation-exchanged sample) crystals possessed an unprecedented shape for γ-MnS nanocrystals, which again demonstrates the powerful synthetic versatility of our cation exchange method. The powder X-ray diffraction (XRD) patterns (Figure S2) clearly depict the evolution of the chemical composition from roxbyite $Cu_7S_4$ (JCPDS No. 23-0958) to metastable γ-MnS (JCPDS No. 40-1289). Notably, the diffraction peaks of NC5 can be well assigned to γ-MnS, indicating that the $Cu_7S_4$ has been almost completely transformed into γ-MnS through cation exchange.

To better resolve the γ-MnS/$Cu_7S_4$ interfaces, we examined the samples by high-resolution TEM (HRTEM, Figure S3) and aberration-corrected high-angle annular dark-field scanning TEM (HAADF-STEM). While the initial template NC1 corresponds to a roxbyite $Cu_7S_4$ single crystal (Figure S4), NC3 contains a well-defined interface between roxbyite $Cu_7S_4$ and γ-MnS (indicated by red dots, Figure 2 a). The lattice fringes with spacings of 1.9 and 3.0 Å in NC3 (Figure 2 b) can be assigned to the (0160) and (101) planes of roxbyite $Cu_7S_4$ and γ-MnS, respectively. Energy-dispersive X-ray spectroscopy (EDS) line scan and mapping analysis further confirmed the heterogeneous nature of the interfaces of the partially cation-exchanged sample (Figure 2 c, d). High-resolution X-ray photoelectron spectroscopy (XPS, Figure S5) by synchrotron radiation ascertained the valence states of $Cu^+$ and $Mn^{2+}$ in the samples.[32,33]

As demonstrated in Figure S6, the combination of roxbyite $Cu_7S_4$ with γ-MnS offers the possibility of harvesting solar light over a broad spectrum ($\lambda > 240$ nm). We thus assessed

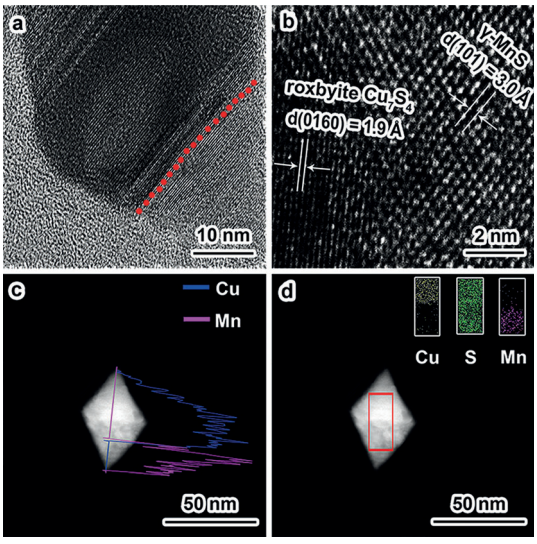


***Figure 2.*** High-resolution electron microscopy of the γ-MnS/$Cu_7S_4$ sample obtained after cation exchange for 1 h (NC3). a) HRTEM image, b) HAADF-STEM image, c) STEM image and EDS line scan profiles, and d) STEM image and EDS mapping profiles.

the performance of our Janus-like γ-MnS/$Cu_7S_4$ structures in photocatalytic $H_2$ production. All of the samples can be readily dispersed in water (Figure S7). The initial evaluation was carried out using $Na_2S/Na_2SO_3$ to quench the photoexcited holes. Under full-spectrum irradiation (Figure 3a), the Janus-like NC3 sample showed the highest $H_2$ production rate of 718 μmol $g^{-1}$ $h^{-1}$, manifesting the function of γ-MnS/$Cu_7S_4$ interfaces in photocatalysis. The apparent quantum efficiency (QE) of $H_2$ production by NC3 at $\lambda = 420$ nm, where both γ-MnS and $Cu_7S_4$ can be photoexcited, was determined to be 18.8%. This efficiency is quite comparable

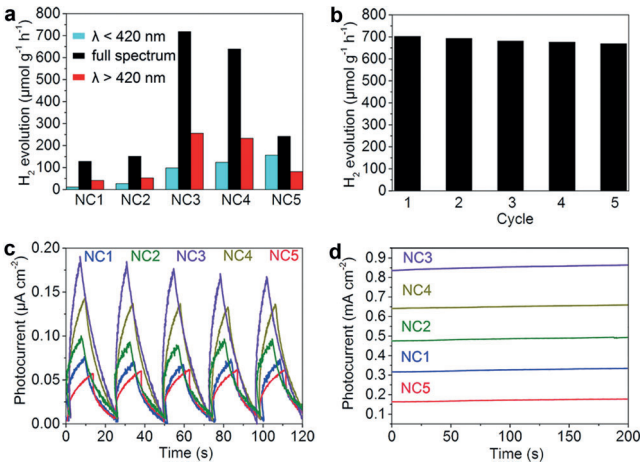


***Figure 3.*** Photocatalytic and PEC measurements. a) Average rates of photocatalytic $H_2$ production with various γ-MnS/$Cu_7S_4$ samples as the catalysts under different light irradiation conditions (full spectrum, $\lambda < 420$ nm, or $\lambda > 420$ nm). b) Photocatalytic cycling tests with an NC3 sample under full-spectrum irradiation. Each cycle was 4 h long. For all of the measurements, the photocatalyst (1 mg) was added to water containing 0.35 M $Na_2S$ and 0.25 M $Na_2SO_3$. c) Photocurrent vs. time (*I–t*) curves for various γ-MnS/$Cu_7S_4$ samples at a bias potential of 0 V vs. Ag/AgCl in 0.5 M $Na_2SO_4$ electrolyte under full-spectrum irradiation. d) PEC *I–t* curves for various γ-MnS/$Cu_7S_4$ samples at a bias potential of 0 V vs. Ag/AgCl under full-spectrum irradiation, recorded in 0.1 M $Na_2S$ and 0.02 M $Na_2SO_3$ solution. The power density for full-spectrum irradiation is 100 mW $cm^{-2}$.

to or exceeds the performance of noble-metal-based photocatalysts.[34] To examine the durability of the catalyst, we conducted five cycles of 4 hours each with NC3 (Figure 3b). The hydrogen production rate remained fairly constant (ca. 700 μmol $g^{-1}$ $h^{-1}$) for 20 hours, demonstrating the high stability of our photocatalytic system.

To further investigate the properties of our Z-scheme photocatalytic water splitting system, we carried out measurements in two different spectral regions, namely the $\lambda < 420$ nm region, which corresponds to the light-harvesting band of γ-MnS, and the $\lambda > 420$ nm region, where $Cu_7S_4$ absorbs. As observed for NC3 and NC4, the photocatalytic $H_2$ production rate for full-spectrum spectrum irradiation was significantly higher than the sum of those obtained under $\lambda < 420$ nm and $\lambda > 420$ nm light irradiation (see Figure 3a). Note that the enhanced activity of pure $Cu_7S_4$ (NC1) under full-spectrum irradiation may be due to the interplay between semiconductor photoexcitation and surface plasmon resonance, which has previously been observed for metal-based plasmonic enhancement.[35] This performance enhancement suggests that the charge generation and separation under full-spectrum irradiation have been substantially improved in the Z-scheme system. This finding was corroborated by photoluminescence (PL) emission spectroscopy (Figure S8). NC3 exhibits the lowest light emission intensity in terms of the characteristic peaks for both $Cu_7S_4$ and γ-MnS among all samples, indicating that the recombination of electron–hole pairs has been substantially suppressed. As for photocatalytic $H_2$ production, photocurrent measurements confirmed that electron–hole separation is most efficient in the properly cation-exchanged NC3 sample (Figure 3c). In such a photoelectrochemical (PEC) cell (Figure S9), unassisted *I–t* measurements showed a stable operation using the samples as the photoelectrodes (Figure 3d),[36] which produced $H_2$ over a Pt cathode (Table S2).

Having investigated the properties of our Z-scheme catalyst, we further determined the energy band structures of our samples by synchrotron radiation photoelectron spectroscopy (SRPES). To simplify these measurements, they were performed on pure $Cu_7S_4$ (NC1) and nearly bare γ-MnS (NC5). The valence band (VB) spectra (Figure 4a) show that the VB edges of $Cu_7S_4$ and γ-MnS are located at 0.16 and 3.92 eV below the Fermi level ($E_F$), respectively. As shown in Figure 4b, the work functions of $Cu_7S_4$ and γ-MnS were calculated from the $E_F$ to be 4.46 and 2.53 eV, respectively. Taken together, $Cu_7S_4$ and γ-MnS have VB edges at −4.61 and −6.45 eV versus the vacuum level, respectively. To determine the conduction band (CB) positions, the optical band gaps were estimated from Tauc plots (Figure 4c), in which $Cu_7S_4$ and γ-MnS were both regarded as

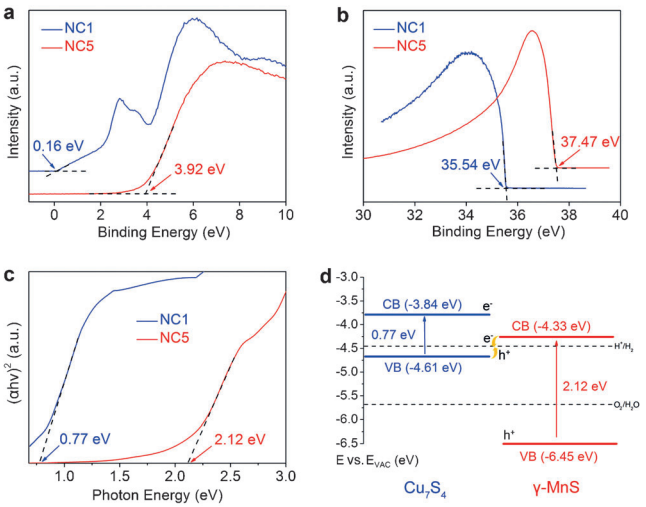


***Figure 4.*** Energy band characterization and diagrams. a) Valence-band spectra obtained by SRPES. b) Secondary electron cutoff ($E_{cutoff}$) of the SRPES spectra ($\lambda_{ex} = 40$ eV). c) Optical band gaps determined by UV/Vis/IR diffuse reflectance spectroscopy (Figure S5). d) The electronic band structures of γ-MnS and $Cu_7S_4$, giving rise to a Z-scheme photocatalyst. e) TEM image of an NC3 sample modified with $MnO_x$. f) Average rates of photocatalytic $H_2$ and $O_2$ production using the NC3/$MnO_x$ catalyst with sacrificial agents (SAs, 0.35 M $Na_2S$ and 0.25 M $Na_2SO_3$) or in overall water splitting (in pure water).

direct band gap materials.[37] As a result, $Cu_7S_4$ and γ-MnS should have the energy band alignment shown in Figure 4d, which can give rise to a valid Z-scheme photocatalytic system.

According to the band structures, this Z-scheme system should be capable of producing both $H_2$ and $O_2$ considering its reduction and oxidation potentials. In fact, photocatalytic $H_2$ production can still take place when the reaction system is placed in pure deionized water and no sacrificial agents are added; however, the production rate was significantly reduced (see Table S3). The major limitation originates from the lack of highly active sites for $O_2$ evolution at the sulfide surface.[38] Our measurements indicate that γ-MnS is the semiconductor limiting the water oxidation process (Table S4). To achieve overall photocatalytic water splitting, we decorated our NC3 nanocrystals with the oxygen-evolution cocatalyst $MnO_x$ using a reported deposition method (Figure 4e).[1,38] The NC3–$MnO_x$ hybrid structures achieved a $H_2$ production rate of 209 $\mu mol\, g^{-1} h^{-1}$ for overall water splitting under full-spectrum irradiation (Figure 4f). The apparent QE of $H_2$ production through water splitting by the NC3–$MnO_x$ at 420 nm is 5.5%. Meanwhile, we also noticed the non-stoichiometric ratio of the $H_2/O_2$ formed in the water splitting process, which was ascribed to the formation of reactive oxygen species alongside $O_2$ production (Figure S10).

In summary, we have synthesized a new noble-metal-free broadband water splitting system by cation exchange, and described our efforts to achieve well-defined interfaces and exposed surfaces towards Z-scheme photocatalysis. This system combines the advantages of broadband light harvesting, efficient charge separation, sufficient band-edge potentials, and low material costs. The strategy reported here enables the seamless integration of two prospective photocatalytic materials at the atomic level. It provides an alternative approach to Z-scheme photocatalysis, and highlights the importance of the development of synthetic methods to the design of photocatalytic materials. Meanwhile, it constitutes another example for the application of cation-exchange synthesis in sustainable energy development.

## Acknowledgements

This work was financially supported in part by the 973 Program (2014CB848900), the NSFC (21471141, U1532135), the CAS Key Research Program of Frontier Sciences (QYZDB-SSW-SLH018), the Recruitment Program of Global Experts, and the CAS Hundred Talent Program. SRPES and XPS experiments were performed at the Catalysis and Surface Science Endstation in the National Synchrotron Radiation Laboratory (NSRL) in Hefei, China.

## Conflict of interest

The authors declare no conflict of interest.

**Keywords:** cation exchange · Janus structures · photocatalysis · water splitting · Z-scheme

[1] A. Iwase, S. Yoshino, T. Takayama, Y. H. Ng, R. Amal, A. Kudo, *J. Am. Chem. Soc.* **2016**, *138*, 10260.
[2] T. T. Zhuang, Y. Liu, Y. Li, Y. Zhao, L. Wu, J. Jiang, S. H. Yu, *Angew. Chem. Int. Ed.* **2016**, *55*, 6396; *Angew. Chem.* **2016**, *128*, 6506.
[3] A. Kudo, Y. Miseki, *Chem. Soc. Rev.* **2009**, *38*, 253.
[4] M. G. Walter, E. L. Warren, J. R. McKone, S. W. Boettcher, Q. Mi, E. A. Santori, N. S. Lewis, *Chem. Rev.* **2010**, *110*, 6446.
[5] A. J. Bard, *J. Photochem.* **1979**, *10*, 59.
[6] H. Tada, T. Mitsui, T. Kiyonaga, T. Akita, J. Tanaka, *Nat. Mater.* **2006**, *5*, 782.
[7] Q. Wang, T. Hisatomi, Q. Jia, H. Tokudome, M. Zhong, C. Wang, Z. Pan, T. Takata, M. Nakabayashi, N. Shibata, Y. Li, I. D. Sharp, A. Kudo, T. Yamada, K. Domen, *Nat. Mater.* **2016**, *15*, 611.
[8] H. Li, W. Tu, Y. Zhou, Z. Zou, *Adv. Sci.* **2016**, *3*, 1500389.
[9] C. Liu, J. Tang, H. M. Chen, B. Liu, P. Yang, *Nano Lett.* **2013**, *13*, 2989.
[10] K. Maeda, *ACS Catal.* **2013**, *3*, 1486.
[11] Y. Tachibana, L. Vayssieres, J. R. Durrant, *Nat. Photonics* **2012**, *6*, 511.
[12] A. Iwase, Y. H. Ng, Y. Ishiguro, A. Kudo, R. Amal, *J. Am. Chem. Soc.* **2011**, *133*, 11054.
[13] K. Iwashina, A. Iwase, Y. H. Ng, R. Amal, A. Kudo, *J. Am. Chem. Soc.* **2015**, *137*, 604.
[14] Z. Chen, F. Bing, Q. Liu, Z. Zhang, X. Fang, *J. Mater. Chem. A* **2015**, *3*, 4652.
[15] H. Yang, S. V. Kershaw, Y. Wang, X. Gong, S. Kalytchuk, A. L. Rogach, W. Y. Teoh, *J. Phys. Chem. C* **2013**, *117*, 20406.
[16] X. Wang, G. Liu, Z. G. Chen, F. Li, L. Wang, G. Q. Lu, H. M. Cheng, *Chem. Commun.* **2009**, 3452.
[17] P. Li, Y. Zhou, H. Li, Q. Xu, X. Meng, X. Wang, M. Xiao, Z. Zou, *Chem. Commun.* **2015**, *51*, 800.
[18] S. Bai, J. Jiang, Q. Zhang, Y. Xiong, *Chem. Soc. Rev.* **2015**, *44*, 2893.
[19] K. Maeda, K. Teramura, D. Lu, N. Saito, Y. Inoue, K. Domen, *Angew. Chem. Int. Ed.* **2006**, *45*, 7806; *Angew. Chem.* **2006**, *118*, 7970.
[20] B. J. Beberwyck, Y. Surendranath, A. P. Alivisatos, *J. Phys. Chem. C* **2013**, *117*, 19759.
[21] L. De Trizio, L. Manna, *Chem. Rev.* **2016**, *116*, 10852.
[22] V. Lesnyak, R. Brescia, G. C. Messina, L. Manna, *J. Am. Chem. Soc.* **2015**, *137*, 9315.
[23] A. E. Powell, J. M. Hodges, R. E. Schaak, *J. Am. Chem. Soc.* **2016**, *138*, 471.
[24] R. Tu, Y. Xie, G. Bertoni, A. Lak, R. Gaspari, A. Rapallo, A. Cavalli, L. De Trizio, L. Manna, *J. Am. Chem. Soc.* **2016**, *138*, 7082.
[25] D. Zhang, A. B. Wong, Y. Yu, S. Brittman, J. Sun, A. Fu, B. Beberwyck, A. P. Alivisatos, P. Yang, *J. Am. Chem. Soc.* **2014**, *136*, 17430.
[26] P. Zhou, J. Yu, M. Jaroniec, *Adv. Mater.* **2014**, *26*, 4920.
[27] Y. Xu, M. A. Schoonen, *Am. Mineral.* **2000**, *85*, 543.
[28] Y. Zheng, Y. Cheng, Y. Wang, L. Zhou, F. Bao, C. Jia, *J. Phys. Chem. B* **2006**, *110*, 8284.
[29] J. Cui, Y. Li, L. Liu, L. Chen, J. Xu, J. Ma, G. Fang, E. Zhu, H. Wu, L. Zhao, L. Wang, Y. Huang, *Nano Lett.* **2015**, *15*, 6295.
[30] D. H. Son, S. M. Hughes, Y. Yin, A. P. Alivisatos, *Science* **2004**, *306*, 1009.
[31] R. D. Robinson, B. Sadtler, D. O. Demchenko, C. K. Erdonmez, L.-W. Wang, A. P. Alivisatos, *Science* **2007**, *317*, 355.

  

[32] J. Lu, P. Qi, Y. Peng, Z. Meng, Z. Yang, W. Yu, Y. Qian, *Chem. Mater.* **2001**, *13*, 2169.
[33] J. Zhang, J. Yu, Y. Zhang, Q. Li, J. R. Gong, *Nano Lett.* **2011**, *11*, 4774.
[34] Z. W. Seh, S. Liu, M. Low, S. Y. Zhang, Z. Liu, A. Mlayah, M. Y. Han, *Adv. Mater.* **2012**, *24*, 2310.
[35] S. K. Cushing, J. Li, F. Meng, T. R. Senty, S. Suri, M. Zhi, M. Li, A. D. Bristow, N. Wu, *J. Am. Chem. Soc.* **2012**, *134*, 15033.
[36] P. Da, M. Cha, L. Sun, Y. Wu, Z.-S. Wang, G. Zheng, *Nano Lett.* **2015**, *15*, 3452.
[37] J. Liu, Y. Liu, N. Liu, Y. Han, X. Zhang, H. Huang, Y. Lifshitz, S.-T. Lee, J. Zhong, Z. Kang, *Science* **2015**, *347*, 970.
[38] R. Li, F. Zhang, D. Wang, J. Yang, M. Li, J. Zhu, X. Zhou, H. Han, C. Li, *Nat. Commun.* **2013**, *4*, 1432.

Manuscript received: January 6, 2017
Final Article published: ■■ ■■, ■■■■

  

# Communications

**Water Splitting**

Q. Yuan, D. Liu, N. Zhang, W. Ye, H. Ju, L. Shi, R. Long, J. Zhu, Y. Xiong* ——— ■■■■–■■■■

Noble-Metal-Free Janus-like Structures by Cation Exchange for Z-Scheme Photocatalytic Water Splitting under Broadband Light Irradiation

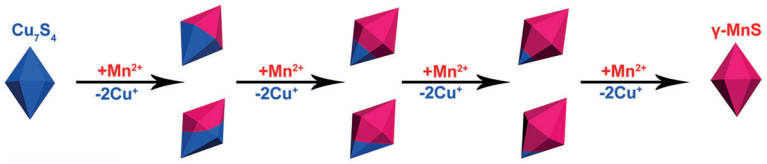


**Janus-like structures** consisting of γ-MnS and $Cu_7S_4$ with high-quality interfaces were obtained by facile cation exchange. The hybrid structures exhibit broadband light absorption and improved charge separation, which led to a hydrogen production rate of 718 $\mu mol\,g^{-1}\,h^{-1}$ under full-spectrum irradiation.

  